FLIGHT DYNAMICS, HANDLING AND RIDE QUALITIES OF A FLEXIBLE AIRCRAFT

A. Khalil, DLR (German Aerospace Center), Institute of Flight Systems
Lilienthalplatz 7, 38108 Braunschweig, Germany

Abstract

The effects of structural flexibility on aircraft flight dynamics and handling qualities are investigated. To do so, the equations of motion of an elastic vehicle are presented and then solved by means of trimming/simulation routines. The simulation results of a linear model are then compared with those of a nonlinear model of DLR's Discus-2c sailplane. To further demonstrate the flexibility effects, two sets of modified aircraft models are developed. The first set alters the modal frequencies of DLR's Discus-2c from their nominal values, whereas the second set alters the modal damping. The handling qualities, in terms of modal criteria and as compared to the MIL-STD-1797A, are examined for the first set of the modified aircraft models. With the second set of the modified aircraft models, the ride qualities in terms of acceleration at pilot location and biodynamic effects are examined.

1. INTRODUCTION

Modern high-efficiency aircraft feature high-aspect-ratio wings, slender fuselages and thin lightweight structures resulting in significant structural flexibility. This flexibility has an effect on the flight dynamics of an aircraft. In their work, Waszak and Schmidt [1] developed an aeroelastic model and applied it for flight dynamics analysis of the Rockwell B-1 bomber aircraft. The mathematical model used the free vibration modes of the aircraft and was represented in the mean-axis system to minimize the inertial coupling. In [2], Schmidt extended the model to cover a large variety of topics on flexible aircraft flight dynamics. In [3], Schmidt and Raney worked together by implementing the same model to predict the effect of flexibility on the handling characteristics of an aircraft. The work used a motion-based flight simulator of NASA Langley Research Center and was applied on two aircraft: the Rockwell B-1 and the Boeing High Speed Civil Transport (HSCT). Raney et al., [4] and [5], extended their work on the HSCT to investigate the effect of flexibility of generic aircraft models on both handling qualities (HQ) and ride qualities (RQ). They did so by means of pilot ratings based on the Cooper-Harper rating scale for HQ and another rating scale for RQ. Mitchell et al., [6], did an excellent review on the evolution and revolution of the handling qualities. They stated that "*There is an impression among the program management community (and, unfortunately, in some disciplines of the engineering community as well) that handling qualities are not an issue today. This impression is wrong*", [6]. This work is intended to study the effects of flexibility on the flight dynamics, HQ and RQ of an aircraft. The example aircraft for this work is DLR's Discus-2c sailplane. The aerodynamic and modal parameters of this sailplane had been identified by Viana, [7], through a series of flight tests. For modal identification, the results of a ground vibration test (GVT) performed on the aircraft by Leichtwerk AG had been used as an initialization for the identification process. The identification was based on the method of Jategaonkar, [8], and used the identification toolbox FITLAB of DLR, [9].

2. THE MATHEMATICAL MODEL

2.1. Rigid-Body Equations of Motion (EOM)

The general equations of unsteady motion of a rigid aircraft can be expressed in the body axis system as in Eq. (1), whereas Eq. (2) represents the rigid-body kinematics equations. And finally, the rate of change of CG position measured with respect to the inertial axis system is given by Eq. (3), see [2]. u, v and w are the translational speeds, p, q and r are the angular speeds, ϕ, θ and ψ are the 3-2-1 Euler angles, x, y and h are the inertial displacements, X, Y and Z are the total external (aerodynamic + propulsive) forces, L, M and N are the total external (aerodynamic + propulsive) moments, m is the aircraft mass, g is Earth's gravity, and finally, I_{**} are the aircraft moments and products of inertia around different axes (* = x, y or z).

$$
\begin{aligned}
& m(\dot{u} + qw - rv) + mg\sin\theta = X \\
& m(\dot{v} + ru - pw) - mg\cos\theta\sin\phi = Y \\
& m(\dot{w} + pv - qu) - mg\cos\theta\cos\phi = Z \\
& I_{xx}\dot{p} - I_{xz}(\dot{r} + pq) - I_{yz}(q^2 - r^2) \\
& \qquad - I_{xy}(\dot{q} - pr) \\
& \qquad + \left(I_{zz} - I_{yy}\right)qr = L \\
& I_{yy}\dot{q} + (I_{xx} - I_{zz})pr - I_{xy}(\dot{p} + qr) \\
& \qquad - I_{yz}(\dot{r} - pq) + I_{xz}(p^2 - r^2) \\
& \qquad = M \\
& I_{zz}\dot{r} - I_{xz}(\dot{p} - qr) - I_{xy}(p^2 - q^2) \\
& \qquad - I_{yz}(\dot{q} + pr) \\
& \qquad + \left(I_{yy} - I_{xx}\right)pq = N
\end{aligned}
\tag{1}
$$

$$(2)\quad \begin{bmatrix}\dot{\phi}\\ \dot{\theta}\\ \dot{\psi}\end{bmatrix}=\begin{bmatrix}1 & sin\phi\, tan\theta & cos\phi\, tan\theta\\ 0 & cos\phi & -sin\phi\\ 0 & sin\phi\, sec\theta & cos\phi\, sec\theta\end{bmatrix}\begin{bmatrix}p\\ q\\ r\end{bmatrix}$$

$$\begin{aligned}(3)\quad \dot{x} &= (cos\theta cos\psi)u + (sin\phi sin\theta cos\psi\\ &\quad - cos\phi sin\psi)v\\ &\quad + (cos\phi sin\theta cos\psi\\ &\quad + sin\phi sin\psi)w\\ \dot{y} &= (cos\theta sin\psi)u + (sin\phi sin\theta sin\psi\\ &\quad + cos\phi cos\psi)v\\ &\quad + (cos\phi sin\theta sin\psi\\ &\quad - sin\phi cos\psi)w\\ \dot{h} &= (sin\theta)u - (sin\phi cos\theta)v - (cos\phi cos\theta)w\end{aligned}$$

2.2. Structural (Elastic) EOM

By using the concept of a lumped-mass vibration structure, the total elastic displacement of that structure expressed in the structural reference axis system might be expressed in terms of modal expansion using n free-vibration modes as in Eq. (4).

$$(4)\quad d_E(x,y,z,t)=\sum_{i=1}^{n}\Phi_i(x,y,z)\eta_i(t)$$

where d_E is the total elastic deformation, Φ_i is the vibration mode shape (eigenfunction), η_i is the generalized coordinate associated with the i^{th} vibration mode. These *n* generalized coordinates are governed by the *n* equations given by Eq. (5), where ζ_i and ω_i are the modal damping and natural frequency, respectively, whereas m_i and Q_i are the generalized mass and force, respectively, each associated with the i^{th} vibration mode.

$$(5)\quad \ddot{\eta}_i + 2\zeta_i\omega_i\dot{\eta}_i + \omega_i^2\eta_i = \frac{Q_i}{m_i}, \qquad i = 1,2,\dots n$$

2.3. Rigid-Body Aerodynamic Model

As noted in Eqs. (1) and (5), the right hand side contains the external forces and moments in addition to the generalized forces. Hence an expression to evaluate these quantities will be provided in this section. The external forces and moments can be represented as in Eq. (6).

$$(6)\quad \begin{aligned} X &= q_\infty S_W C_X, & L &= q_\infty S_W b C_l\\ Y &= q_\infty S_W C_Y, & M &= q_\infty S_W c C_m\\ Z &= q_\infty S_W C_Z, & N &= q_\infty S_W b C_n\end{aligned}$$

where q_∞, S_W, b and c are the dynamic pressure, wing planform area, wing span and wing mean aerodynamic chord, respectively. The coefficients C_X, C_Y and C_Z are the longitudinal, side and vertical force coefficients, respectively, whereas C_l, C_m and C_n are the rolling, pitching and yawing moment coefficients, respectively. The longitudinal and vertical force coefficients can be represented by means of a 2-point model - fuselage/wing (FW) and horizontal tail (HT) - through Eq. (7).

$$(7)\quad \begin{aligned} C_X &= C_{X(FW)} + C_{X(HT)}\\ C_Z &= C_{Z(FW)} + C_{Z(HT)}\end{aligned}$$

The FW and HT force coefficients are related to the lift and drag coefficients through Eqs. (8) and (9), respectively.

$$(8)\quad \begin{aligned} C_{X(FW)} &= C_{L(FW)}\sin(\alpha) - C_{D(FW)}\cos(\alpha)\\ C_{Z(FW)} &= -C_{L(FW)}\cos(\alpha) - C_{D(FW)}\sin(\alpha)\end{aligned}$$

$$\begin{aligned}(9)\quad C_{X(HT)} &= C_{L(HT)}\sin(\alpha_H - i_H)\\ &\quad - C_{D(HT)}\cos(\alpha_H - i_H)\\ C_{Z(HT)} &= -C_{L(HT)}\cos(\alpha_H - i_H)\\ &\quad - C_{D(HT)}\sin(\alpha_H - i_H)\end{aligned}$$

where α is the aircraft angle of attack and α_H and i_H are the local angle of attack and incidence angle of the horizontal tail, respectively. The horizontal tail local angle of attack at time *t* is given by Eq. (10).

$$(10)\quad \alpha_H(t) = \alpha(t) - \varepsilon(t-\tau_\varepsilon) + i_H + \alpha_{dyn}(t)$$

where $\alpha_{dyn} = \tan^{-1} qr_H/V_\infty$ is the change of local angle of attack of the horizontal tail due to aircraft pitch rotation, r_H is the distance between the aerodynamic center (AC) of the horizontal tail and the aircraft CG, and ε is the downwash angle which can be expressed as in Eq. (11).

$$\begin{aligned}(11)\quad \varepsilon(t-\tau_\varepsilon) &= \varepsilon_0 + \frac{\partial\varepsilon}{\partial\alpha}\alpha(t) - \frac{\partial\varepsilon}{\partial\alpha}\dot{\alpha}(t)\frac{r_H^*}{V_\infty}\\ &\quad + \frac{\partial\varepsilon}{\partial X}[1 - X(t-\tau_\varepsilon)]\end{aligned}$$

where $\tau_\varepsilon(= r_H^*/V_\infty)$ represents a time delay for the shed vortex until reaching the horizontal tail AC, r_H^* is the distance between wing AC and horizontal tail AC, V_∞ is the true airspeed, and $X(t)$ is the wing upper surface instantaneous location of flow separation along its chord delayed by τ_ε. An extension to this 2-point aerodynamic model will be used here. The extension is based on [7] and uses a 3-point model: fuselage/right wing (FWR), fuselage/left wing (FWL), and horizontal tail (HT). The longitudinal aerodynamic coefficients, namely, C_L, C_D and C_m will be affected by lateral-directional motion and control variables. An expression for the lift coefficient can be given as in Eq. (12), where * means *R* or *L*, S_H is the horizontal tail planform area, and δ_e, δ_a $\left(=\frac{\delta_a^R - \delta_a^L}{2}\right)$ and δ_a^{sym} $(=\frac{\delta_a^R + \delta_a^L}{2})$ are the elevator, aileron and symmetric aileron control surface deflections, respectively. The term $C_{L_{QSSF}}(=$

$\left\{\frac{1+\sqrt{X(t)}}{2}\right\}^2$) represents the reduction of the lift curve slope at high angles of attack. The term $X(t)(=\frac{1}{2}\{1-tanh[a_1(\alpha(t)-\tau_2\dot{\alpha}(t)-\alpha^*)]\})$ is as defined previously, where a_1 is the airfoil static stall characteristic, τ_2 is a hysteresis time constant, and α^* is a breakpoint. An expression for the drag coefficient can be given as in Eq. (13).

$$
\begin{aligned}
&C_{L(FW*)}(t)\\
&= C_{L_0(FW*)} + \frac{1}{2}C_{L_\alpha(FW)}C_{L_{QSSF}(FW)}(t)\alpha(t)\\
&+ \frac{1}{2}C_{L_q(FW)}\frac{q(t)c}{2V_\infty(t)} + C_{L_{\beta^2(FW*)}}\beta^2(t)\\
&+ C_{L_{\delta_a^2}(FW*)}\delta_a^2(t)\\
&+ \left[C_{L_{\delta_a^{sym}(FW*)}} + C_{L_{\alpha\delta_a^{sym}(FW*)}}\alpha(t)\right]\delta_a^{sym}(t)
\end{aligned}
\tag{12}
$$

$$
\begin{aligned}
C_{L(HT)}(t) &= \frac{S_H}{S_W}\Big[C_{L_\alpha(HT)}\alpha_H(t)\\
&\quad + C_{L_{\delta_e}(HT)}\delta_e(t)\Big]\cos(\alpha_{dyn}(t)\\
&\quad - \varepsilon(t-\tau_\varepsilon))
\end{aligned}
$$

$$
\begin{aligned}
C_{L(FW)}(t) &= C_{L(FWR)}(t) + C_{L(FWL)}(t)\\
C_L(t) &= C_{L(FW)}(t) + C_{L(HT)}(t)
\end{aligned}
$$

$$
\begin{aligned}
C_{D(FW)}(t) &= C_{D_0(FW)} + k_1 C_{L(FW)}(t)\\
&\quad + \frac{\left[C_{L(FW)}(t) + C_{L(HT)}(t)\right]^2}{e\pi AR}\\
&\quad + C_{D_{\beta^2(FW)}}\beta^2(t)\\
&\quad + C_{D_{\delta_a^2(FW)}}\delta_a^2(t)\\
&\quad + \left[C_{D_{\delta_a^{sym}(FW)}}\right.\\
&\quad \left. + C_{D_{\alpha\delta_a^{sym}(FW)}}\alpha(t)\right]\delta_a^{sym}(t)\\
&\quad + C_{D_{QSSF(FW)}}(t)
\end{aligned}
\tag{13}
$$

$$
\begin{aligned}
C_{D(HT)}(t) &= \frac{S_H}{S_W}k_2 C_{L(HT)}(t)\\
C_D(t) &= C_{D(FW)}(t) + C_{D(HT)}(t)
\end{aligned}
$$

The pitching moment coefficient around the wing AC is given by Eq. (14). And finally, transforming the pitching moment coefficient from AC to CG is given by Eq. (15). Similar expressions for the lateral-directional coefficients expressed at AC can be derived as in Eqs. (16), (17) and (18), where VT is the vertical tail and δ_r is the rudder control surface deflection; whereas their transformation to CG is given by Eq. (19).

$$
\begin{aligned}
C^{AC}_{m(FW*)}(t) &= C_{m_{0(FW*)}}\\
&\quad + \frac{1}{2}\Big(C_{m_{q(FW)}}\\
&\quad + C_{m_{q\alpha(FW)}}\alpha(t)\Big)\frac{q(t)c}{2V_\infty(t)}\\
&\quad + C_{m_{\beta^2(FW*)}}\beta^2(t)\\
&\quad + C_{m_{\delta_a^2(FW*)}}\delta_a^2(t)\\
&\quad + C_{m_{p(FW*)}}\frac{p(t)b}{2V_\infty(t)}\\
&\quad + C_{m_{r(FW*)}}\frac{r(t)b}{2V_\infty(t)}\\
&\quad + \frac{1}{2}C_{m_{QSSF(FW)}}(t)\\
&\quad + \Big[C_{m_{\delta_a^{sym}(FW*)}}\\
&\quad + C_{m_{\alpha\delta_a^{sym}(FW*)}}\alpha(t)\Big]\delta_a^{sym}(t)
\end{aligned}
\tag{14}
$$

$$
\begin{aligned}
C^{AC}_{m(HT)}(t) &= -\frac{r_H^*}{c}\frac{S_H}{S_W}C_{L(HT)}(t)\\
C^{AC}_{m(FW)}(t) &= C^{AC}_{m(FWR)}(t) + C^{AC}_{m(FWL)}(t)\\
C^{AC}_{m}(t) &= C^{AC}_{m(FW)}(t) + C_{m(HT)}(t)
\end{aligned}
$$

$$
\begin{aligned}
C^{CG}_m(t) &= C^{AC}_m(t) + \left[C_{Z(FW)}(t)\right.\\
&\quad \left. + C_{Z(HT)}(t)\right]\frac{x_{CG}-x_{AC}}{c}\\
&\quad - \left[C_{X(FW)}(t)\right.\\
&\quad \left. + C_{X(HT)}(t)\right]\frac{z_{CG}-z_{AC}}{c}
\end{aligned}
\tag{15}
$$

$$
\begin{aligned}
C^{AC}_{l(FW*)}(t) &= C_{l_{0(FW*)}} + C_{l_{\beta(FW*)}}\beta(t)\\
&\quad + C_{l_{\dot{\beta}(FW*)}}\frac{\dot{\beta}(t)b}{2V_\infty(t)}\\
&\quad + C_{l_{\beta\alpha(FW*)}}\beta(t)\alpha(t)\\
&\quad + C_{l_{p(FW*)}}\frac{p(t)b}{2V_\infty(t)}\\
&\quad + C_{l_{p\alpha(FW*)}}\frac{p(t)b}{2V_\infty(t)}\alpha(t)\\
&\quad + C_{l_{r(FW*)}}\frac{r(t)b}{2V_\infty(t)}\\
&\quad + C_{l_{r\alpha(FW*)}}\frac{r(t)b}{2V_\infty(t)}\alpha(t)\\
&\quad + C_{l_{\delta_a(FW*)}}\delta_a(t)\\
&\quad + C_{l_{\delta_a\alpha(FW*)}}\delta_a(t)\alpha(t)
\end{aligned}
\tag{16}
$$

$$
\begin{aligned}
C^{AC}_{l(VT)}(t) &= C_{l_{\delta_r(VT)}}\delta_r(t) + C_{l_{\delta_r\alpha(VT)}}\delta_r(t)\alpha(t)\\
C^{AC}_{l(FW)}(t) &= C^{AC}_{l(FWR)}(t) + C^{AC}_{l(FWL)}(t)\\
C^{AC}_{l}(t) &= C^{AC}_{l(FW)}(t) + C^{AC}_{l(VT)}(t)
\end{aligned}
$$

$$
\begin{aligned}
C_Y(t) &= C_{Y_0} + C_{Y_\beta}\beta(t) + C_{Y_{\dot{\beta}}}\frac{\dot{\beta}(t)b}{2V_\infty(t)}\\
&\quad + C_{Y_p}\frac{p(t)b}{2V_\infty(t)} + C_{Y_r}\frac{r(t)b}{2V_\infty(t)}\\
&\quad + C_{Y_{\delta_a}}\delta_a(t) + C_{Y_{\delta_r}}\delta_r(t)
\end{aligned}
\tag{17}
$$

$$
\begin{aligned}
C_n^{AC}(t) = {} & C_{n_0} + C_{n_\beta}\beta(t) + C_{n_{\dot\beta}}\frac{\dot\beta(t)b}{2V_\infty(t)} \\
& + C_{n_{\beta\alpha}}\beta(t)\alpha(t) \\
& + C_{n_p}\frac{p(t)b}{2V_\infty(t)} \\
& + C_{n_{p\alpha}}\frac{p(t)b}{2V_\infty(t)}\alpha(t) \\
& + C_{n_r}\frac{r(t)b}{2V_\infty(t)} \\
& + C_{n_{r\alpha}}\frac{r(t)b}{2V_\infty(t)}\alpha(t) \\
& + C_{n_{\delta_a}}\delta_a(t) + C_{n_{\delta_r}}\delta_r(t) \\
& + C_{n_{\delta_r\alpha}}\delta_r(t)\alpha(t)
\end{aligned}
\tag{18}
$$

$$
\begin{aligned}
C_l^{CG}(t) &= C_l^{AC}(t) + C_Y^{CG}(t)\frac{z_{CG} - z_{AC}}{b} \\
C_n^{CG}(t) &= C_n^{AC}(t) + C_Y^{CG}(t)\frac{x_{CG} - x_{AC}}{b}
\end{aligned}
\tag{19}
$$

2.4. Flexible-Body Aerodynamic Model

In this section, the effect of flexibility on the aerodynamic model will be presented. This effect is shown in two ways: 1) the effect of flexibility on the total external (aerodynamic + propulsive) forces and moments (see Eqs. (20) and (21)) and 2) the effect of rigid-body motion on generalized coordinates, which appear in the generalized forces (see Eqs. (22) and (23)).

$$
\begin{aligned}
X &= X^R + X^F, & L &= L^R + L^F \\
Y &= Y^R + Y^F, & M &= M^R + M^F \\
Z &= Z^R + Z^F, & N &= N^R + N^F
\end{aligned}
\tag{20}
$$

where again X, Y, Z, L, M and N are as defined before as the external forces and moments, where now the superscripts *R* and *F* are for rigid and flexible bodies, respectively. The rigid parts of them had been previously defined by the rigid-body aerodynamic model and will not be altered due to flexibility. The flexible external forces and moments can be defined analogously to Eq. (6), where now the flexible aerodynamic coefficients are defined by Eq. (21), where l is a characteristic length being equal to c for symmetric modes and b for antisymmetric ones. The generalized forces are divided, as in Eqs. (22) and (23), into two parts: 1) rigid-flexible (RF), 2) flexible-flexible (FF).

2.5. Aeroelastic Model

By using the mean axis system (one at which the relative translational and angular momenta about the center of mass resulting from elastic deformation of a structure undergoing free vibration diminish), the equations of motion of the rigid body and the structural vibrations become uncoupled (except for the external forces and moments and the generalized forces). Hence, the aeroelastic model is constituted of Eqs. (1), (2), (3) and (5) in addition to those of the rigid- and flexible-body aerodynamic models. These equations are 12+*n* in number, have 12+2*n* states, and are nonlinear and coupled differential equations of first and second order.

$$
\begin{aligned}
C_X^F &= \sum_{i=1}^{n} C_{X_{\eta_i}}\eta_i + \sum_{i=1}^{n} C_{X_{\dot\eta_i}}\frac{\dot\eta_i l}{2V_\infty} \\
C_Y^F &= \sum_{i=1}^{n} C_{Y_{\eta_i}}\eta_i + \sum_{i=1}^{n} C_{Y_{\dot\eta_i}}\frac{\dot\eta_i l}{2V_\infty} \\
C_Z^F &= \sum_{i=1}^{n} C_{Z_{\eta_i}}\eta_i + \sum_{i=1}^{n} C_{Z_{\dot\eta_i}}\frac{\dot\eta_i l}{2V_\infty} \\
C_l^F &= \sum_{i=1}^{n} C_{l_{\eta_i}}\eta_i + \sum_{i=1}^{n} C_{l_{\dot\eta_i}}\frac{\dot\eta_i l}{2V_\infty} \\
C_m^F &= \sum_{i=1}^{n} C_{m_{\eta_i}}\eta_i + \sum_{i=1}^{n} C_{m_{\dot\eta_i}}\frac{\dot\eta_i l}{2V_\infty} \\
C_n^F &= \sum_{i=1}^{n} C_{n_{\eta_i}}\eta_i + \sum_{i=1}^{n} C_{n_{\dot\eta_i}}\frac{\dot\eta_i l}{2V_\infty}
\end{aligned}
\tag{21}
$$

$$
Q_i = Q_i^{RF} + Q_i^{FF}, \qquad i = 1,2,\dots n \tag{22}
$$

$$
\begin{aligned}
Q_i^{RF} = {} & q_\infty S_W l\left(C_0^{\eta_i} + C_\alpha^{\eta_i}\alpha + C_\beta^{\eta_i}\beta + C_p^{\eta_i}\frac{pb}{2V_\infty}\right. \\
& + C_q^{\eta_i}\frac{qc}{2V_\infty} + C_r^{\eta_i}\frac{rb}{2V_\infty} + C_{\delta_a}^{\eta_i}\delta_a \\
& + C_{\delta_e}^{\eta_i}\delta_e + C_{\delta_r}^{\eta_i}\delta_r \\
& \left. + C_{\delta_a^{sym}}^{\eta_i}\delta_a^{sym}\right), i = 1,2,\dots n \\
Q_i^{FF} = {} & q_\infty S_W l\left(\sum_{j=1}^{n} C_{\eta_j}^{\eta_i}\eta_j\right. \\
& \left. + \sum_{i=1}^{n} C_{\dot\eta_j}^{\eta_i}\frac{\dot\eta_j l}{2V_\infty}\right), i = 1,2,\dots n
\end{aligned}
\tag{23}
$$

2.6. Observation Equations

Until now, the presented equations of motion are expressed with regard to the mean axis system. Nevertheless, for a comparison with flight test data, all measured quantities should be corrected for rigid displacement away from aircraft CG and also for structural motion. The true airspeed of an aircraft is calculated as in Eq. (24). The static temperature, static pressure and density may be calculated as in Eq. (25), where h_0, T_{s_0} and p_{s_0} are the reference altitude, static temperature and static pressure (usually those at sea level), respectively; $\frac{dT}{dh}$ is the temperature gradient of the standard atmosphere ($-0.0065\ \mathrm{K/m}$ for the troposphere), R is the air gas constant ($287.058\ \mathrm{J/(kg\,K)}$) and g_0 is the gravity at sea level ($9.80665\ \mathrm{m/s^2}$).

$$V = \sqrt{u^2 + v^2 + w^2} \tag{24}$$

$$\begin{aligned} T_s &= T_{s_0} + \frac{dT}{dh}(h - h_0) \\ p_s &= p_{s_0}\left(\frac{T_s}{T_{s_0}}\right)^{-\frac{g_0}{\frac{dT}{dh}R}} \\ \rho &= \frac{p_s}{RT_s} \end{aligned} \tag{25}$$

Since the angle of attack and the sideslip angle are typically measured at a location which is displaced from the aircraft CG by (x_{NB}, y_{NB}, z_{NB}), the velocity components will be given as in Eq. (26). Hence, the measured angle of attack and sideslip angle can be calculated as in Eq. (27). In addition, the angular rates and angular accelerations will also be affected by the structural deformation as given in Eqs. (28) and (29), respectively.

$$\begin{aligned} u_{NB} &= u + qz_{NB} - ry_{NB} \\ v_{NB} &= v + rx_{NB} - pz_{NB} \\ w_{NB} &= w + py_{NB} - qx_{NB} \end{aligned} \tag{26}$$

$$\begin{aligned} \alpha_{NB} &= \tan^{-1}\frac{w_{NB}}{u_{NB}} \\ \beta_{NB} &= \sin^{-1}\frac{v_{NB}}{\sqrt{u_{NB}^2 + v_{NB}^2 + w_{NB}^2}} \end{aligned} \tag{27}$$

$$\begin{aligned} p_{IMU} &= p + \dot{v}_x^{IMU} = p + \sum_{i=1}^{n} v_{x,\eta_i}^{IMU}\dot{\eta}_i \\ q_{IMU} &= q + \dot{v}_y^{IMU} = q + \sum_{i=1}^{n} v_{y,\eta_i}^{IMU}\dot{\eta}_i \\ r_{IMU} &= r + \dot{v}_z^{IMU} = r + \sum_{i=1}^{n} v_{z,\eta_i}^{IMU}\dot{\eta}_i \end{aligned} \tag{28}$$

$$\begin{aligned} \dot{p}_{IMU} &= \dot{p} + \ddot{v}_x^{IMU} = \dot{p} + \sum_{i=1}^{n} v_{x,\eta_i}^{IMU}\ddot{\eta}_i \\ \dot{q}_{IMU} &= \dot{q} + \ddot{v}_y^{IMU} = \dot{q} + \sum_{i=1}^{n} v_{y,\eta_i}^{IMU}\ddot{\eta}_i \\ \dot{r}_{IMU} &= \dot{r} + \ddot{v}_z^{IMU} = \dot{r} + \sum_{i=1}^{n} v_{z,\eta_i}^{IMU}\ddot{\eta}_i \end{aligned} \tag{29}$$

3. SOLUTION OF THE EOM

In this section, the 12+n nonlinear and coupled differential equations will be solved for an arbitrary control surface input. But before doing so, they will be solved for trim at a given steady flight condition. After solving for trim, the nonlinear equations can be dissolved into steady equations plus small perturbations (linear differential equations) added to them.

where $v_{x,\eta_i}^{IMU}, v_{y,\eta_i}^{IMU}, and\ v_{z,\eta_i}^{IMU}$ are the rotations of the i^{th} mode at the IMU location due to structural deformation around respective axes. The Euler angles at the IMU location are given as in Eq. (30), where $\Delta\phi_{IMU}, \Delta\theta_{IMU}$ and $\Delta\psi_{IMU}$ represent the changes in Euler angles due to structural deformation measured at the IMU location (see Eq. (31)), which is the same transformation as that from angular rates to Euler angle rates.

$$\begin{aligned} \phi_{IMU} &= \phi + \Delta\phi_{IMU} \\ \theta_{IMU} &= \theta + \Delta\theta_{IMU} \\ \psi_{IMU} &= \psi + \Delta\psi_{IMU} \end{aligned} \tag{30}$$

$$\begin{bmatrix} \Delta\phi_{IMU} \\ \Delta\theta_{IMU} \\ \Delta\psi_{IMU} \end{bmatrix} = \begin{bmatrix} 1 & sin\phi\ tan\theta & cos\phi\ tan\theta \\ 0 & cos\phi & -sin\phi \\ 0 & sin\phi\ sec\theta & cos\phi\ sec\theta \end{bmatrix} \begin{bmatrix} v_{x,\eta_i}^{IMU} \\ v_{y,\eta_i}^{IMU} \\ v_{z,\eta_i}^{IMU} \end{bmatrix} \tag{31}$$

In case of using an accelerometer located at $(x_{acc}, y_{acc}, z_{acc})$, the measured acceleration is related to the acceleration of the aircraft CG through Eq. (32), where the acceleration of the aircraft CG is given by Eq. (33).

$$\begin{aligned} a_x^{acc} &= a_x^{CG} - x_{acc}(q^2 + r^2) + y_{acc}(pq - \dot{r}) \\ &\quad + z_{acc}(pr + \dot{q}) + \sum_{i=1}^{n} \Phi_{x,\eta_i}^{acc}\ddot{\eta}_i \\ a_y^{acc} &= a_y^{CG} - x_{acc}(pq + \dot{r}) - y_{acc}(p^2 + r^2) \\ &\quad + z_{acc}(qr - \dot{p}) + \sum_{i=1}^{n} \Phi_{y,\eta_i}^{acc}\ddot{\eta}_i \\ a_z^{acc} &= a_z^{CG} - x_{acc}(pr - \dot{q}) + y_{acc}(qr + \dot{p}) \\ &\quad - z_{acc}(p^2 + q^2) + \sum_{i=1}^{n} \Phi_{z,\eta_i}^{acc}\ddot{\eta}_i \end{aligned} \tag{32}$$

$$\begin{aligned} a_x^{CG} &= \dot{u} + qw - rv + g\sin\theta \\ a_y^{CG} &= \dot{v} + ru - pw - g\sin\phi\cos\theta \\ a_z^{CG} &= \dot{w} + pv - qu - g\cos\phi\cos\theta \end{aligned} \tag{33}$$

3.1. The Trim Problem

The aircraft will be trimmed for two steady flight conditions: 1) steady rectilinear flight, 2) steady coordinated turn. The aircraft to be trimmed in this work is a sailplane with no engine and it has an aerodynamic asymmetry (e.g. lateral-directional aerodynamic biases).

3.1.1. Steady Rectilinear Flight

This flight condition is defined as in Table 1.

3.1.2. Steady Coordinated Turn

This flight condition is defined as in Table 2. The equations given by Eq. (34), see [10], are used as initial values for ϕ, p, q and r for trimming.

$$
\begin{aligned}
\phi &= \frac{\dot{\psi} V_\infty}{g \cos\theta} \\
p &= -\dot{\psi} \sin\theta \\
q &= \dot{\psi} \sin\phi \cos\theta \\
r &= \dot{\psi} \cos\phi \cos\theta
\end{aligned} \tag{34}
$$

Table 1 Trim for Steady Rectilinear Flight

Model	Trim requirements	Trim variables	Fixed states and control deflections
Rigid	V_∞	u, v, w	h, ϕ, ψ
	$\dot{u} = \dot{v} = \dot{w} = 0$	p, q, r	δ_a^{sym}
	$\dot{p} = \dot{q} = \dot{r} = 0$	θ	
	$\dot{\phi} = \dot{\theta} = \dot{\psi} = 0$	$\delta_a, \delta_e, \delta_r$	
Flexible	V_∞	u, v, w	h, ϕ, ψ
	$\dot{u} = \dot{v} = \dot{w} = 0$	p, q, r	δ_a^{sym}
	$\dot{p} = \dot{q} = \dot{r} = 0$	θ	
	$\dot{\phi} = \dot{\theta} = \dot{\psi} = 0$	$\delta_a, \delta_e, \delta_r$	
	$\ddot{\eta}_i = 0$	η_i	

Table 2 Trim for Steady Coordinated Turn

Model	Trim requirements	Trim variables	Fixed states and control deflections
Rigid	$V_\infty, \beta, \dot{\psi}$	u, v, w	h, ψ
	$\dot{u} = \dot{v} = \dot{w} = 0$	p, q, r	δ_a^{sym}
	$\dot{p} = \dot{q} = \dot{r} = 0$	ϕ, θ	
	$\dot{\phi} = \dot{\theta} = 0$	$\delta_a, \delta_e, \delta_r$	
Flexible	$V_\infty, \beta, \dot{\psi}$	u, v, w	h, ψ
	$\dot{u} = \dot{v} = \dot{w} = 0$	p, q, r	δ_a^{sym}
	$\dot{p} = \dot{q} = \dot{r} = 0$	ϕ, θ	
	$\dot{\phi} = \dot{\theta} = 0$	$\delta_a, \delta_e, \delta_r$	
	$\ddot{\eta}_i = 0$	η_i	

3.2. Nonlinear Simulation

After successfully trimming the aircraft at the required steady flight condition, the nonlinear and coupled equations of motion can then be solved for arbitrary control surface inputs by means of a numerical integration technique (e.g. fourth-order Runge-Kutta), with the initial conditions to be those resulting from the trim. In case of a rigid aircraft, the generalized coordinates and their first derivatives $(\eta_i, \dot{\eta}_i)$ are set to zero without altering the identified aerodynamic parameters.

3.3. Stability Assessment

The nonlinear and coupled equations can now be linearized around the trimmed state leading to a set of linear differential equations which can be used to numerically obtain the Jacobian which is required for stability assessment, classical flight control design, and also for linear simulations. For a general nonlinear system, as given by Eq. (35), an equivalent linear system, as in Eq. (36), can be obtained, which gives a good approximation of the original nonlinear system around a trimmed (equilibrium) state (x_0, u_0, y_0), where $\delta_x(t)(= x(t) - x_0)$ is the perturbation state vector, $\delta_u(t)(= u(t) - u_0)$ is the perturbation input vector, and $\delta_y(t)(= y(t) - y_0)$ is the perturbation output vector.

$$
\begin{aligned}
\dot{x}(t) &= f\big(x(t), u(t)\big), \qquad x(0) = \bar{x} \\
y(t) &= g(x(t), u(t))
\end{aligned} \tag{35}
$$

$$
\begin{aligned}
\dot{\delta}_x(t) &= A\delta_x(t) + B\delta_u(t), \quad \delta_x(0) = 0 \\
\delta_y(t) &= C\delta_x(t) + D\delta_u(t)
\end{aligned} \tag{36}
$$

The matrices A, B, C and D are four Jacobian matrices which are numerically calculated as given by Eq. (37) with finite differences approximating the partial derivatives.

$$
\begin{aligned}
A &:= \left.\frac{\partial f}{\partial x}\right|_{\substack{x=x_0 \\ u=u_0}}, \quad B := \left.\frac{\partial f}{\partial u}\right|_{\substack{x=x_0 \\ u=u_0}} \\
C &:= \left.\frac{\partial g}{\partial x}\right|_{\substack{x=x_0 \\ u=u_0}}, \quad D := \left.\frac{\partial g}{\partial u}\right|_{\substack{x=x_0 \\ u=u_0}}
\end{aligned} \tag{37}
$$

In case of flexible aircraft, the state vector is normally composed of ten of the twelve rigid-body

states $(u, v(or\ \beta), w(or\ \alpha), p, q, r, \phi, \theta, \psi, h)$ and the generalized coordinates and their first derivatives $(\eta_i, \dot{\eta}_i)$. In this case, the whole system can be partitioned as in Eqs. (38) and (39), [2].

$$\begin{aligned} &\begin{Bmatrix} \dot{x}_R \\ \dot{x}_E \end{Bmatrix} = A \begin{Bmatrix} x_R \\ x_E \end{Bmatrix} + Bu \\ &y = C \begin{Bmatrix} x_R \\ x_E \end{Bmatrix} + Du \end{aligned} \tag{38}$$

$$\begin{aligned} &A = \begin{bmatrix} A_R & A_{ER} \\ A_{RE} & A_E \end{bmatrix}, \quad B = \begin{bmatrix} B_R \\ B_E \end{bmatrix} \\ &C = \begin{bmatrix} C_R & C_E \end{bmatrix} \end{aligned} \tag{39}$$

The stability of such a linear system can be easily determined by evaluating the eigenvalues of the A matrix. In case of rigid aircraft, the eigenvalues of the A_R matrix are evaluated, which gives the classical longitudinal (phugoid and short period) and lateral-directional (spiral, Dutch roll, and pure rolling) modes. The matrix A_{ER} represents the effect of flexibility on rigid-body motion (due to the additive external flexible forces and moments to the rigid-body ones), whereas the matrix A_{RE} represents the effect of rigid-body motion on structural vibration (due to the rigid-flexible part of the generalized forces). Since, in general, these two matrices are not zeros, it is expected that the rigid-body modes will be different from those of the whole flexible system.

4. SIMULATION RESULTS

4.1. The Aircraft

The aircraft used for both flight test and simulation is DLR's Discus-2c (Fig. 1), which is a high-performance single-seat sailplane manufactured by Schempp-Hirth Flugzeugbau GmbH. The aircraft has the general mass and geometry characteristics given in Table 3. The modal characteristics of the aircraft are given in Table 4. A flight test measurement system was installed by messWERK GmbH to the aircraft. It includes: 5-hole probe nose boom, thermometer, GPS, INS, wire sensor on air brake (control input position), angle sensor on all control surfaces, and a data acquisition system.

4.2. Phugoid Stabilization

It has been found that the phugoid mode is unstable. Since DLR's pilots did not like that, DLR is considering installing a phugoid stabilizer (a feedback controller, Fig. 4) on the Discus-2c for further flight tests. In the remainder of this paper results are shown for the aircraft with a first version of this phugoid stabilizer.

4.3. Exemplary Results

For some selected maneuvers simulation results are plotted in Fig. 2 (elevator input) and Fig. 3 (rudder input). The results show a good match between the nonlinear (which had been verified with the flight test data by Viana, [7]) and linear models. Hence, both the linear and nonlinear flexible models can be used in case of handling and ride qualities assessment and structural/gust load alleviation control system design.

3.4. Linear Simulation

By expressing the whole system in a set of linear differential equations, a linear simulation can now be performed. The results of this linear simulation (which represents the perturbation quantities) when added to their respective trim quantities, will give the total simulation results (that could be compared with those of the nonlinear simulation).

Fig. 1 DLR's Discus-2c Sailplane in Flight

Table 3 Discus-2c Geometry and Mass Characteristics

Parameter	Value
Geometry	
c [m]	0.685
b [m]	18
S_W [m^2]	11.39
Mass and Inertia	
m (with pilot 1 or 2) [kg]	451 or 422
I_{xx} [kg m^2]	3190
I_{yy} [kg m^2]	870
I_{zz} [kg m^2]	3900
$I_{xy} = I_{yz} = I_{xz}$	0

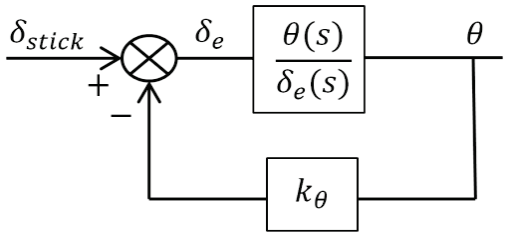

Fig. 4 Phugoid Stabilization Block Diagram

Table 4 DLR's Discus-2c Modal Characteristics (in vacuum)

Mode	Description	Gen. mass [kg cm^2]	Freq. [rad/s]	Damp. ratio
1	**1st Symmetric mode** (wing vertical bending)	20	16.02	0
2	**2nd Symmetric mode** (wing in-plane bending)	19.85	30.52	0
3	**3rd Symmetric mode** (wing vertical bending)	10.35	48.59	0
4	**1st Antisymmetric mode** (fuselage bending and wing vertical and in-plane bending)	18.55	30.04	0
5	**2nd Antisymmetric mode** (fuselage torsion and rotation of the horizontal tail)	3.50	32.31	0
6	**3rd Antisymmetric mode** (fuselage torsion and wing vertical and in-plane bending)	14.85	37.37	0

5. FLEXIBILITY EFFECTS

5.1. The Modified Aircraft Models

To further investigate the effect of flexibility, some modified aircraft models are developed. Since the flexibility is inversely proportional to the square of the modal frequencies, see [11], the first set of the modified aircraft models is obtained by decreasing selected modal frequencies of the baseline Discus-2c aircraft by a frequency ratio. This is equivalent to increasing the flexibility of the aircraft, Table 5. While doing this alteration of the modal frequencies, both the aerodynamic parameters and the mass and inertia properties are assumed to be the same as those of the baseline aircraft. The objective of this set is to investigate the effect of flexibility on handling qualities. A second set of modified aircraft models, Table 6, is obtained by increasing the modal damping. The objective of this set is to investigate the damping effect on ride qualities in terms of acceleration at pilot location and also the biodynamic effects resulting from the cross-coupling of accelerations. The investigation was performed at four flight conditions, Table 7.

Table 6 2nd Set of the Modified Aircraft Models

Model	Affected Mode	Modal Damp. [-]	
		baseline	damp
damp	1st Antisymmetric + 2nd Antisymmetric + 3rd Antisymmetric	0	0.07
damp+	1st Antisymmetric + 2nd Antisymmetric + 3rd Antisymmetric	0	0.15
damp++	1st Antisymmetric + 2nd Antisymmetric + 3rd Antisymmetric	0	0.3

Table 7 Flight Conditions

FC	h [m]	V_{TAS} [km/hr]	q_∞ [N/m^2]	V_{EAS} [km/hr]
1	3000	100	351	86.1
2	1000	100	429	95.2
3	3000	160	898	137.8
4	1000	160	1098	152.4

Table 5 1st Set of the Modified Aircraft Models

Model	Affected Mode(s)	Frequency Ratio	Flexibility Ratio	Modal Frequencies [rad/s]	
				baseline	flex
flex1	1st Symmetric + 3rd Symmetric (wing vertical bending)	0.85	1.38	16.02 / 48.59	13.62 / 41.30
flex1+	1st Symmetric + 3rd Symmetric (wing vertical bending)	0.7	2.04	16.02 / 48.59	11.21 / 34.01
flex2	2nd Symmetric mode (wing in-plane bending)	0.85	1.38	30.52	25.94
flex2+	2nd Symmetric mode (wing in-plane bending)	0.7	2.04	30.52	21.36

5.2. Handling Qualities (HQ)

For handling qualities assessment, the military standard MIL-STD-1797A, [12], is used. Only the pitch-axis criteria are addressed here. And since the phugoid mode had been stabilized with a damping ratio that satisfies Level 1 handling qualities, only the short-period mode is considered here. To do so, a low-order equivalent system (LOES) should be obtained and matched with the high-order system (HOS) simultaneously for both the elevator-to-pitch-rate and elevator-to-normal-acceleration-load-factor-at-CG transfer functions. Since the HOS only arises due to the flexible modes (i.e., no higher-order flight control system), an LOES is being obtained by model reduction that retains only the static-elastic deflections (i.e., $\dot{\eta}_i = 0, \ddot{\eta}_i = 0$). The frequency response of the elevator-to-pitch-rate transfer function, Fig. 5, shows an almost perfect match between the HOS and LOES (since the pitch rate at the CG location is almost unaffected by the structural dynamics). Also Fig. 6 shows a good match between the HOS and LOES in the frequency range less than that of the structural modes for the elevator-to-normal-acceleration-load-factor-at-CG transfer function. Fig. 7 shows the mismatch at one of the flight conditions as compared to the envelopes of maximum unnoticeable added dynamics of the MIL-STD-1797A. It shows a good match between the HOS and the LOES. DLR's Discus-2c aircraft is categorized as Class 1 (Small Light Aircraft) and the Flight Phase Category B (cruise) is of typical interest. As a consequence, the Control Anticipation Parameter (CAP) or $\frac{\omega_{sp}}{n/\alpha}$ and short period damping ζ_{sp} are defined as in Fig. 8, where $\frac{n}{\alpha} = \frac{V_0}{g}\frac{1}{T_{\theta_2}}$ and T_{θ_2} is the time constant of the zero corresponding to the short period mode. The time delay τ_{e_θ} is zero, which is Level 1. The variation in handling qualities of the 1st set of the modified aircraft models is shown in Fig. 9 and Fig. 10. As can be noted, the variation in the HQ is small as the aircraft still satisfies Level 1 requirements.

5.3. Ride Qualities (RQ)

The RQ in terms of acceleration at the pilot location is an important aspect when dealing with flexible aircraft. Fig. 11 shows such an acceleration for a rudder sweep input of DLR's Discus-2c aircraft. In this maneuver, the pilot was asked to give only a rudder sweep input, but as can be seen he also gave both aileron and elevator inputs at almost the same frequency as that of the rudder input (from time 30 to 38 seconds). This occurred because he was holding the stick while giving the rudder input, which resulted in a phenomenon known as biodynamic coupling (transfer of aircraft dynamics to pilot's hands). In order to decrease/eliminate this biodynamic coupling and also to enhance the ride qualities, the increase of modal damping could be a useful technique. Fig. 12 shows the power spectral density (PSD) of the acceleration at the pilot location for the 2nd set of the modified aircraft models. The maximum lateral acceleration at the pilot location has been attenuated to almost the half by increasing the modal damping from 0 to 0.3. Of course such a high modal damping of the structural modes might only be achievable in practice by means of an active modal suppression flight control system, if at all.

CONCLUSIONS, RECOMMENDATIONS, AND FUTURE WORK

- The low-order equivalent system obtained in this paper can be used for handling qualities (HQ) assessment and stability augmentation system control design for the rigid-body dynamics. Both, the linear and nonlinear flexible models can additionally be used in case of ride qualities (RQ) assessment and structural/gust load alleviation control system design.
- For the type of aircraft presented here, i.e. a large sailplane, the HQ had not been altered too much by changing the structural flexibility, whereas the RQ had been greatly influenced by changing the structural damping.
- While using the modified aircraft models, the aerodynamic coefficients and mass/inertia properties were assumed not to be altered, which is of course not the real situation. Also, the current HQ criteria assume a frequency separation between the rigid- and flexible-body modes. Hence, to further investigate the effects of structural flexibility, it is suggested to develop a variable-flexibility aircraft concept (in contrast to variable stability or Total In-Flight Simulators used for HQ criteria development).
- As part of the work done on DLR's Discus-2c sailplane, a structural load monitoring model had been developed. This model is planned to be used, together with the flight dynamics model presented here, for the design of a structural/gust load alleviation control system. It is also planned to implement and flight-test the resulting control system.

ACKNOWLEDGMENT

Many thanks to Dipl.-Ing. Per Ohme and Dr.-Ing. Holger Duda for their continuous help and support. Also thanks to Dipl.-Ing. Wulf Mönnich, Dr.-Ing. Marcus Viana and Dipl.-Ing. Christian Raab for their helpful discussions.

REFERENCES

[1] M. R. Waszak and D. K. Schmidt, "Flight Dynamics of Aeroelastic Vehicles," *AIAA J. AIRCRAFT,* vol. 25, no. 6, 1988.

[2] D. K. Schmidt, Modern Flight Dynamics, 1st ed., McGraw-Hill, 2011.

[3] D. K. Schmidt and D. L. Raney, "Modeling and Simulation of Flexible Flight Vehicles," *AIAA JOURNAL OF GUIDANCE, CONTROL, AND DYNAMICS,* vol. 24, no. 3, 2001.

[4] D. L. Raney, E. B. Jackson, C. S. Buttrill and W. M. Adams, "The Impact of Structural Vibration on Flying Qualities of a Supersonic Transport," in *AIAA Atmospheric Flight Mechanics*, Montreal, Canada, 2001.

[5] D. L. Raney, E. B. Jackson and C. S. Buttrill, "Simulation Study of Impact of Aeroelastic Characteristics on Flying Qualities of a High Speed Civil Transport," NASA TP-211943, October 2002.

[6] D. G. Mitchell, D. B. Doman, D. L. Key, D. H. Klyde, D. B. Leggett, D. J. Moorhouse, D. H. Mason, D. L. Raney and D. K. Schmidt, "Evolution, Revolution, and Challenges of Handling Qualities," *AIAA JOURNAL OF GUIDANCE, CONTROL, AND DYNAMICS,* vol. 27, no. 1, 2004.

[7] M. V. P. Viana, "Time-Domain System Identification of Rigid-Body Multipoint Loads Model," in *AIAA Atmospheric Flight Mechanics Conference*, Washington, D.C., 2016.

[8] R. V. Jategaonkar, Flight Vehicle System Identification: A Time-Domain Methodology, 2nd ed., AIAA, Progress in Astronautics and Aeronautics, Volume 245, 2015.

[9] S. Seher-Weiß, "FitlabGui - a Versatile Tool for Data Analysis, System Identification and Helicopter Handling Qualities Analysis," in *42nd European Rotorcraft Forum*, Lille, France, 2016.

[10] F. L. L. E. N. J. Brian L. Stevens, Aircraft Control and Simulation: Dynamics, Controls Design, and Autonomous Systems, Third Edition, Wiley-Blackwell, 2016.

[11] A. K. Pandey and M. Biswas, "Damage Detection in Structures Using Changes in Flexibility," *Journal of Sound and Vibration,* vol. 169, no. 1, pp. 3-17, January 1994.

[12] "Flying Qualities of Piloted Aircraft, MIL-STD-1797A Notice 3," Department of Defense, 2004.

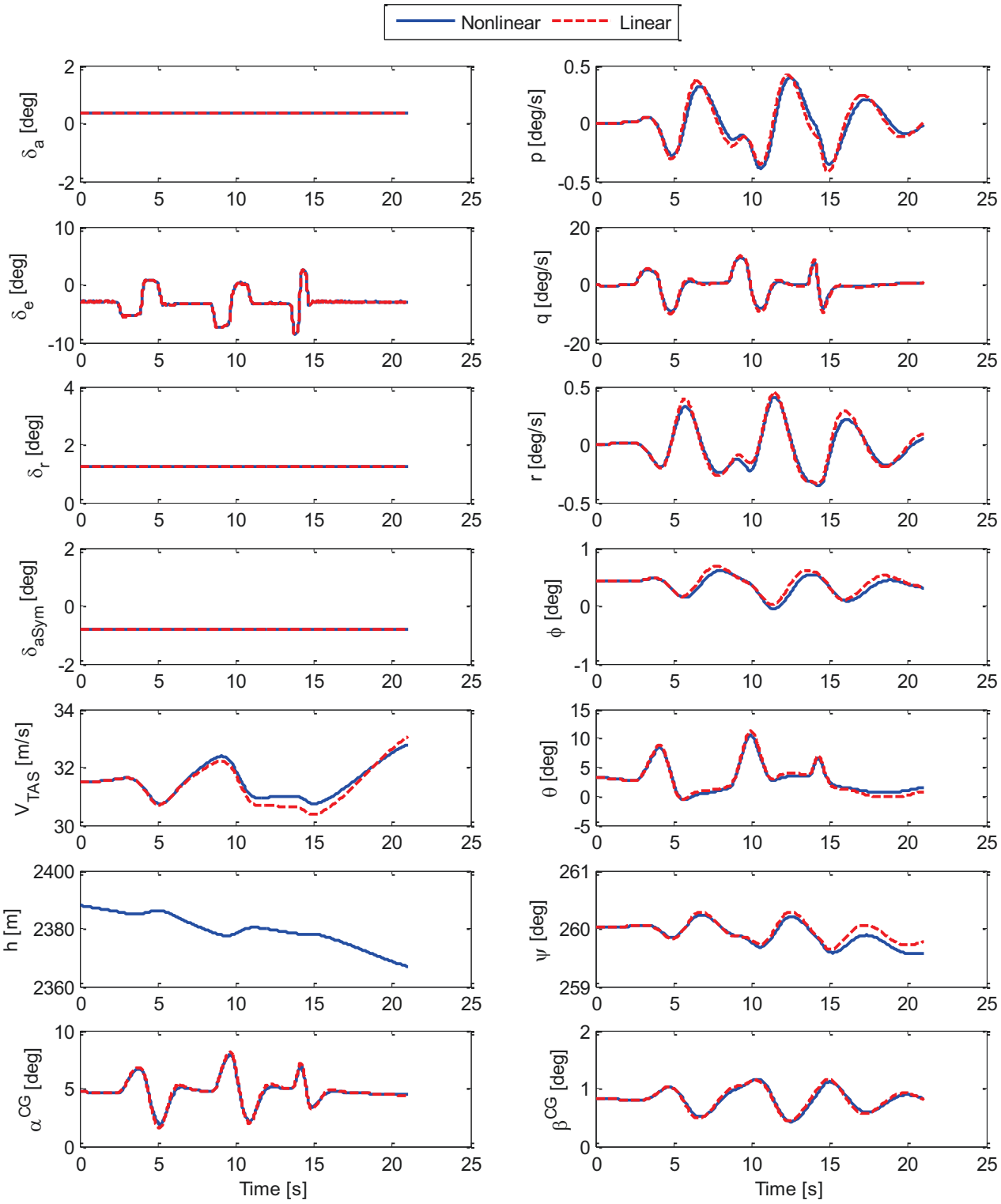

Fig. 2 Compound Elevator Doublet

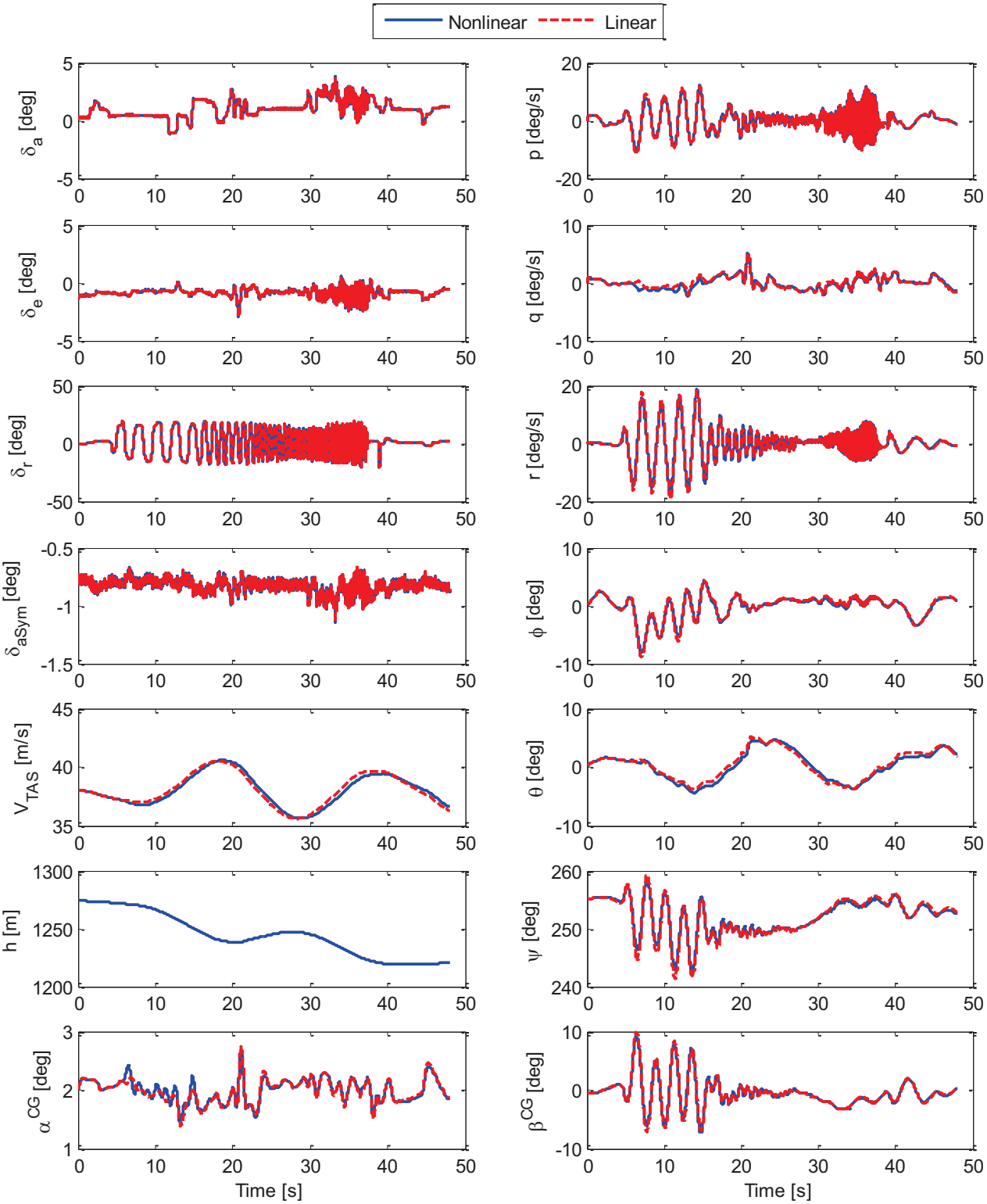

Fig. 3 Rudder Sweep

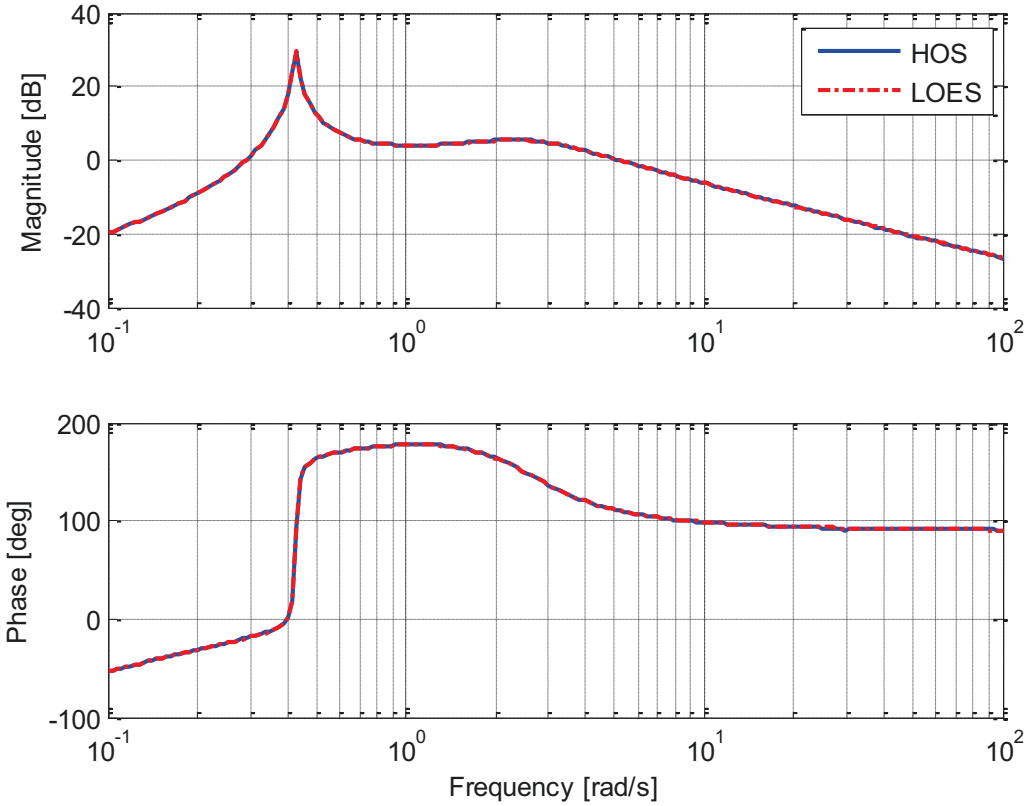

Fig. 5 Elevator to Pitch-Rate Bode Plot

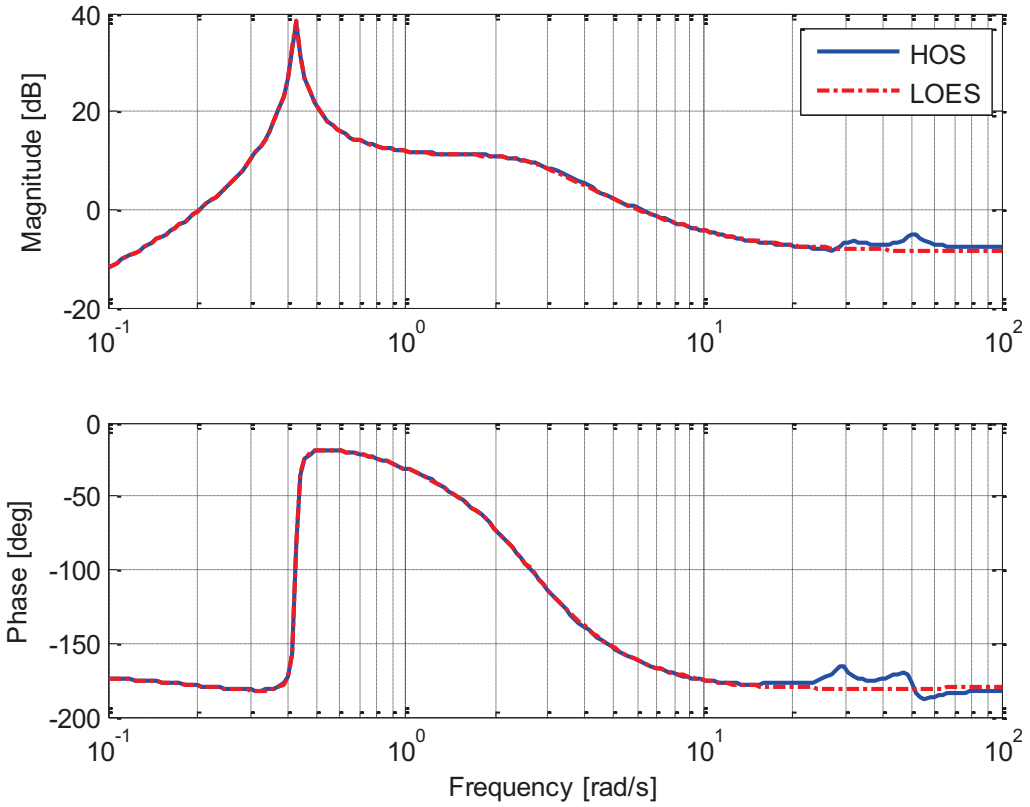

Fig. 6 Elevator to Normal-Acceleration-Load-Factor-at-CG Bode Plot

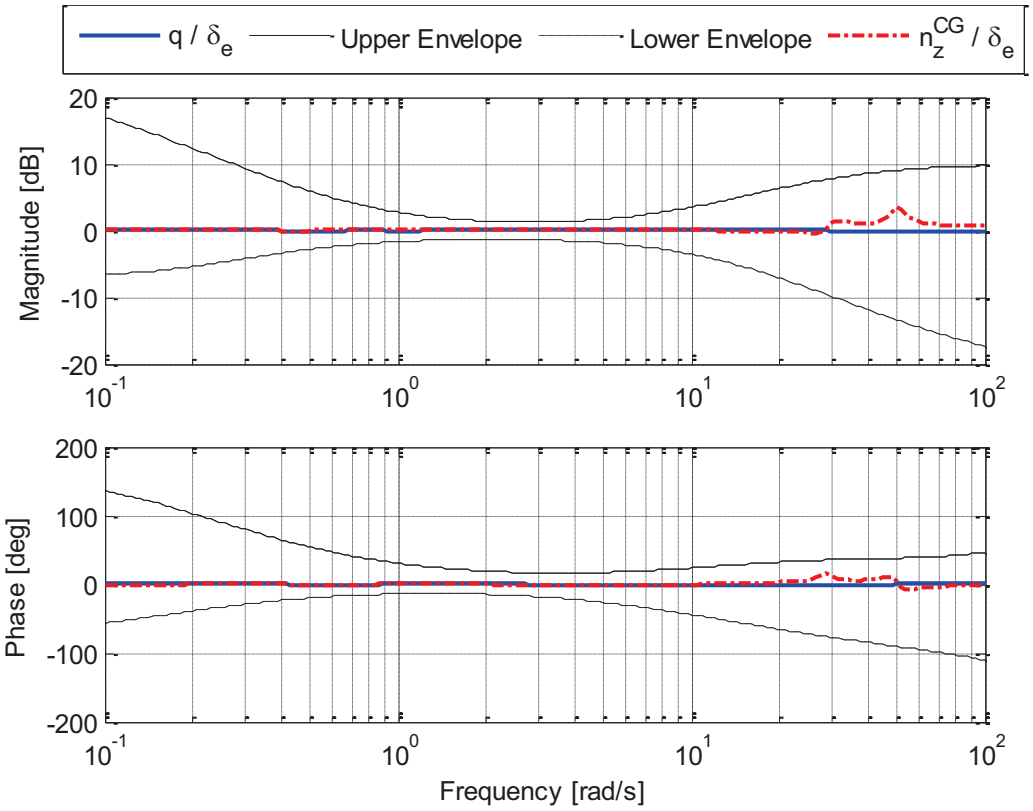

Fig. 7 Mismatch between HOS and LOES within the Envelopes of Maximum Unnoticeable Added Dynamics

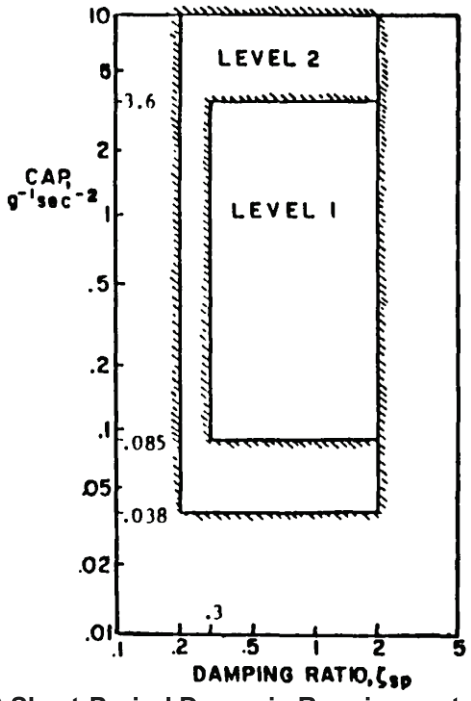

Fig. 8 Short-Period Dynamic Requirements from MIL-STD-1797A

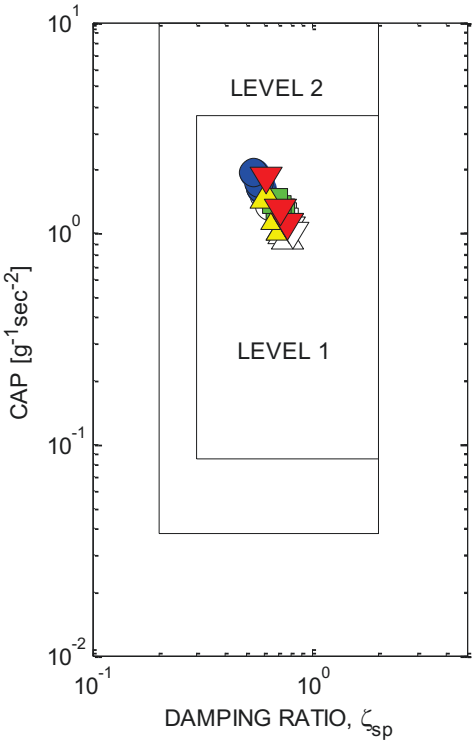

Fig. 9 Short-Period HQ Variation of the 1st Set of the Modified Aircraft Models (See also Fig. 10)

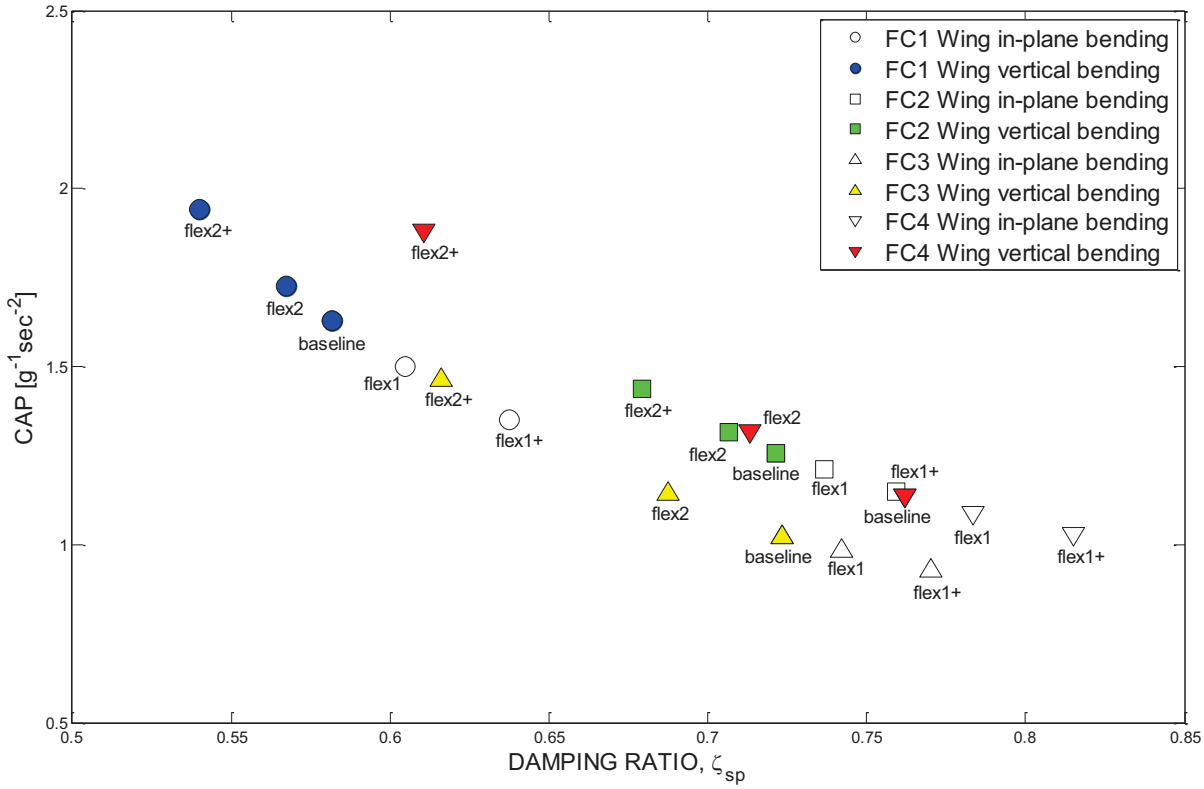

Fig. 10 Short-Period HQ Variation of the 1st Set of the Modified Aircraft Models (Reproduced from Fig. 9)

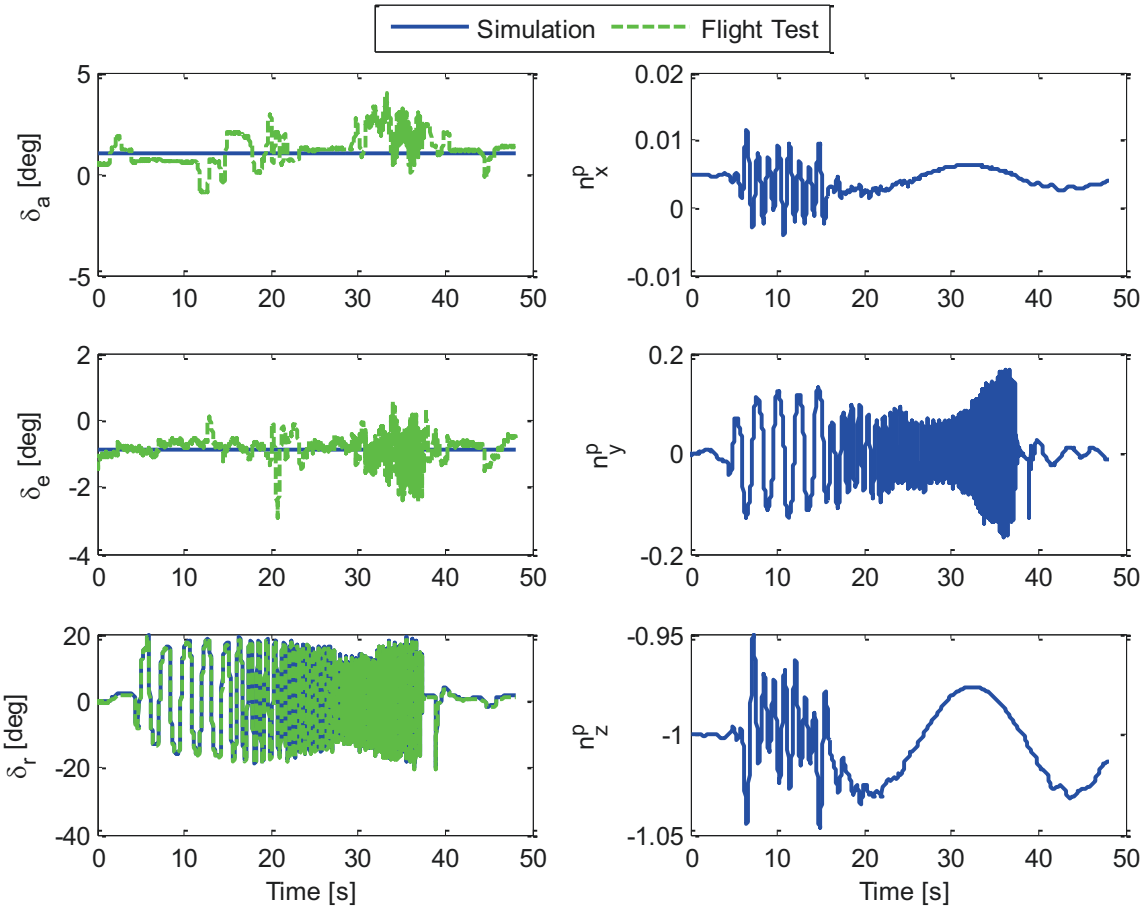

Fig. 11 Rudder Sweep with Biodynamic Coupling

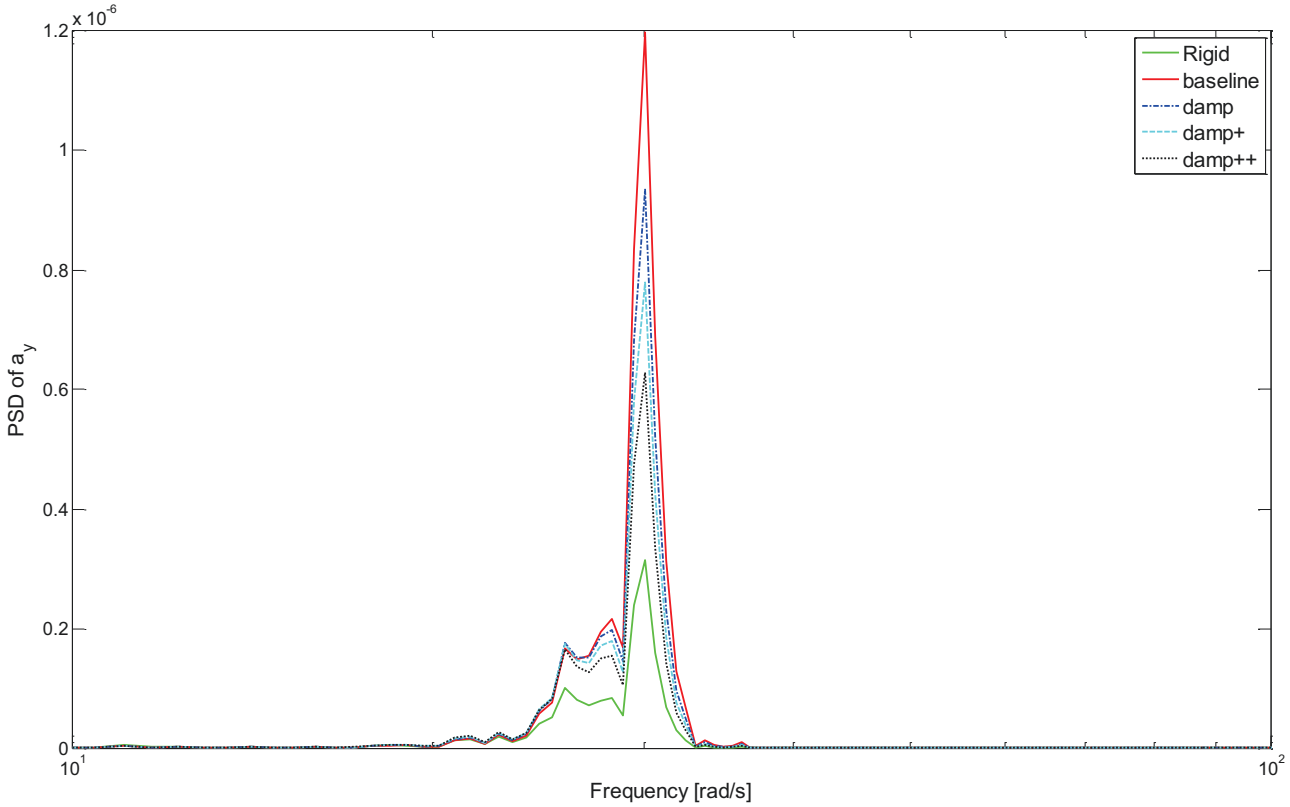

Fig. 12 Power Spectral Density of Lateral Acceleration at Pilot Location